Electronic Supplementary Information

Single-molecule magnet properties of a monometallic dysprosium pentalene complex

Alexander F. R. Kilpatrick,[a] Fu-Sheng Guo,[b] Benjamin M. Day,[b]
Akseli Mansikkamäki,*[c] Richard A. Layfield*[a] and F. Geoffrey N. Cloke*[a]

[a]Department of Chemistry, School of Life Sciences, University of Sussex,
Brighton, BN1 9QJ, UK.

[b]School of Chemistry, The University of Manchester, Manchester, M13 9PL, U.K.

[c]Department of Chemistry, Nanoscience Center, University of Jyväskylä,
P.O. Box 35, Jyväskylä, FI-40014, Finland.

Experimental: general considerations

All manipulations were carried out using standard Schlenk techniques under argon, or in an MBraun glovebox under an inert atmosphere of nitrogen or argon. All glassware was dried at 160°C overnight prior to use. Solvents were purified by pre-drying over sodium wire and then distilled over Na (toluene), K (THF, hexane) or Na-K alloy (pentane) under nitrogen. Dried solvents were collected, degassed and stored over argon in K mirrored ampoules, except THF which was stored in ampoules containing activated 4 Å molecular sieves. Deuterated solvent (C_6D_6) was degassed by three freeze-pump-thaw cycles, dried by refluxing over potassium for three days, vacuum distilled into ampoules and stored under nitrogen. $K_2Pn^{\dagger}$ was prepared according to a published procedure.[1] $DyCl_3$ was prepared by dehydration of $DyCl_3{\cdot}6H_2O$ with excess Me_3SiCl in refluxing heptane over three days. Anhydrous YCl_3 was kindly donated by co-workers.

NMR spectra were measured on Varian VNMRS 400 (^{1}H 399.5 MHz; ^{13}C{^{1}H} 100.25 MHz; ^{29}Si{^{1}H} 79.4 MHz) or VNMRS 500 (^{1}H 499.9 MHz; ^{13}C{^{1}H} 125.7 MHz) spectrometers. The spectra were referenced internally to the residual protic solvent (^{1}H) or the signals of the solvent (^{13}C). ^{29}Si NMR spectra were referenced externally relative to $SiMe_4$. Mass spectra were recorded by Dr A. Abdul-Sada at the University of Sussex using a VG Autospec Fisons instrument (electron ionisation at 70 eV). Elemental analyses for all compounds were carried out by Mr S. Boyer at the Elemental Analysis Service, London Metropolitan University.

Magnetic measurements were carried out using Quantum Design MPMS-7 or MPMP3 SQUID magnetometers at temperatures in the range 1.8-300 K. The samples were prepared in the glovebox by restraining a crystalline sample in eicosane, contained in an NMR tube sealed with a J. Young valve. The samples were then placed under vacuum and flame-sealed. Values of the magnetic susceptibility were corrected for the underlying diamagnetic increment by using tabulated Pascal constants, and the effect of the blank sample holders (gelatin capsule/straw).

Single crystal X-ray diffraction data for $\mathbf{1_{Dy}}$ and $\mathbf{1_Y}$ were collected on an Agilent Technologies Xcalibur Gemini Ultra diffractometer (CuKα source, λ = 1.54184 Å) equipped with a Eos CCD area detector. The data were collected at 173 K using an Oxford Cryosystems Cobra low temperature device. Data were processed using CrysAlisPro (version 1.171.36.32),[2] and unit cell parameters were refined against all data. An empirical absorption correction was carried out using the MULTI-SCAN program.[3] Structures were solved using DIRDIF-2008[4] or SUPERFLIP[5] and refined on Fo2 by full-matrix least-squares refinements using SHELXL-2013.[6] Solutions and refinements were performed using the Olex2[7] or WinGX[8] packages and software packages within. All non-hydrogen atoms were refined with anisotropic displacement parameters. All hydrogen atoms parameters were constrained. For both $\mathbf{1_{Dy}}$ and $\mathbf{1_Y}$ the Cp* ligand (C27 to C36) was positionally disordered over two sites. The disorder was modelled adequately by splitting the Me groups (C32 to C36) over two positions. For $\mathbf{1_{Dy}}$, restrain instructions were applied to give the thermal parameters more reasonable values, and the distance C31-C36A was restrained to prevent serious CheckCIF alerts.

Synthesis of $\mathbf{1_{Dy}}$

A solution of $K_2Pn^{\dagger}$ (590 mg, 1.20 mmol) in THF (20 mL) was added dropwise to a suspension of $DyCl_3$ (322 mg, 1.20 mmol) in THF (40 mL) and stirred for three hours. Solid NaCp* (189 mg, 1.19 mmol) was added slowly and the resulting orange mixture was stirred at room temperature for 12 hours, then at 75°C for three hours. The solvent was removed *in vacuo* and the residues were extracted with hexane (3 × 10 mL) and filtered through Celite on a frit. The filtrate was stripped to dryness and the crude orange solids were recrystallised from pentane at −35 °C. Total yield: 290 mg (34% with respect to $K_2Pn^{\dagger}$). EI-MS: *m/z* = 712 (100%), $[M]^+$; 669 (25%), $[M - {}^{i}Pr]^+$; 577 (20%), $[M - Cp^*]^+$. Anal. found (calcd. for $C_{36}H_{61}DySi_2$): C, 60.52 (60.68); H, 8.72 (9.62)%.

Synthesis of $\mathbf{1_Y}$

Following a procedure analogous to the preparation of $\mathbf{1_{Dy}}$ starting from YCl_3 (153 mg, 0.784 mmol) afforded $\mathbf{1_Y}$ in 30% yield. X-ray quality crystals were grown from a saturated pentane-toluene solution (10:1 v/v) at −35 °C. ^{1}H NMR (C_6D_6, 399.5 MHz, 303 K): δ_H 6.74 (2H, dd, J_{YH} = 1.1, $^3J_{HH}$ = 3.0 Hz, Pn *H*), 5.40 (2H, d, $^3J_{HH}$ = 3.1 Hz, Pn *H*), 1.96 (15H, s, Cp* C*H*$_3$), 1.26 (6H, m, ^{i}Pr C*H*), 1.15 (18H, d, $^3J_{HH}$ = 7.2 Hz, ^{i}Pr CH_3), 1.03 (18H, d, $^3J_{HH}$ = 7.3 Hz, ^{i}Pr CH_3). $^{13}C\{^1H\}$ NMR (C_6D_6, 125.7 MHz, 303 K): δ_C 147.1 (d, J_{YC} = 3.2 Hz, Pn bridgehead *C*), 131.8 (d, J_{YC} = 1.4 Hz, Pn *C*H), 119.5 (d, J_{YC} = 1.8 Hz, Pn *C*H), 103.1 (s, Cp* *C*CH_3), 98.48 (d, J_{YC} = 1.7 Hz, Pn *C*-Si), 19.68 (s, ^{i}Pr *C*H_3), 19.47 (s, ^{i}Pr CH_3), 12.76 (s, ^{i}Pr *C*H), 11.50 (s, Cp*-C*C*H_3). $^{29}Si\{^1H\}$ NMR (C_6D_6, 79.4 MHz, 303 K): δ_{Si} 1.98. EI-MS: *m/z* = 639 (100%), $[M]^+$. Anal. found (calcd. for $C_{36}H_{61}Si_2Y$): C, 67.51 (67.67); H, 9.58 (9.62) %.

Synthesis of Dy@$\mathbf{1_Y}$

The magnetic site 20-fold diluted sample was synthesised by combination of the crude solids $\mathbf{1_Y}$ and $\mathbf{1_{Dy}}$ in a 20:1 molar ratio, followed by recrystallisation from pentane at −35 °C. Accurate dysprosium/yttrium ratios were measured by inductively coupled plasma atomic emission (ICP) spectroscopy using a Thermo iCap 6300 ICP-OES instrument, which resulted in a dysprosium content of 5.0±0.5%.

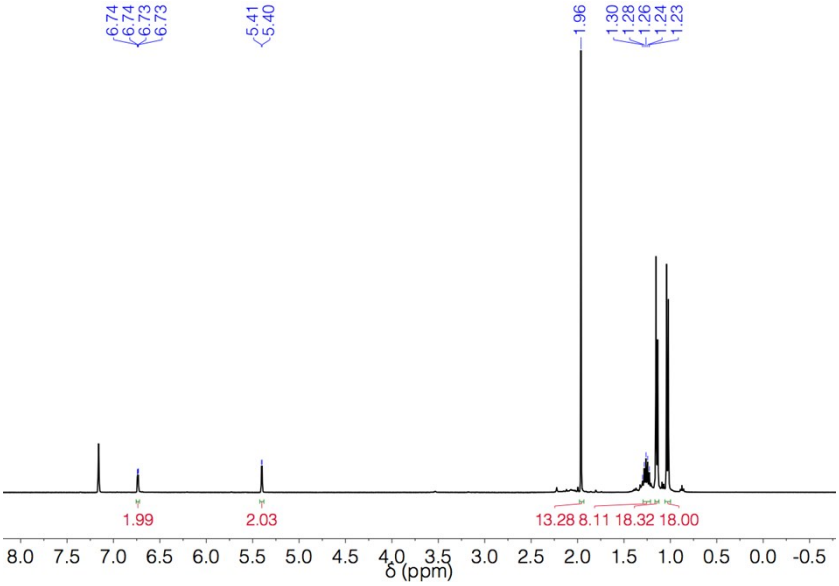

Figure S1 ^{1}H NMR spectrum (C_6D_6, 399.5 MHz, 303 K) of $\mathbf{1_Y}$.

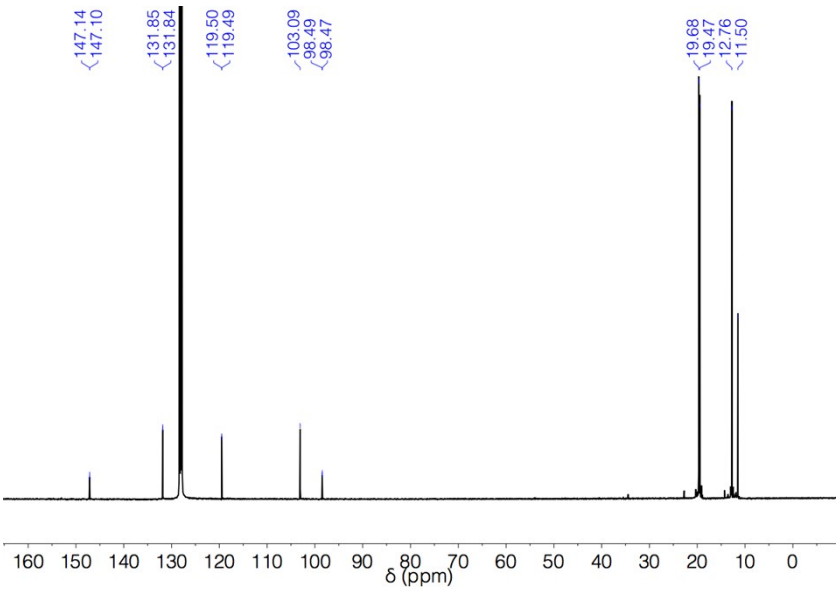

Figure S2 ^{13}C NMR spectrum (C_6D_6, 125.7 MHz, 303 K) of $\mathbf{1_Y}$.

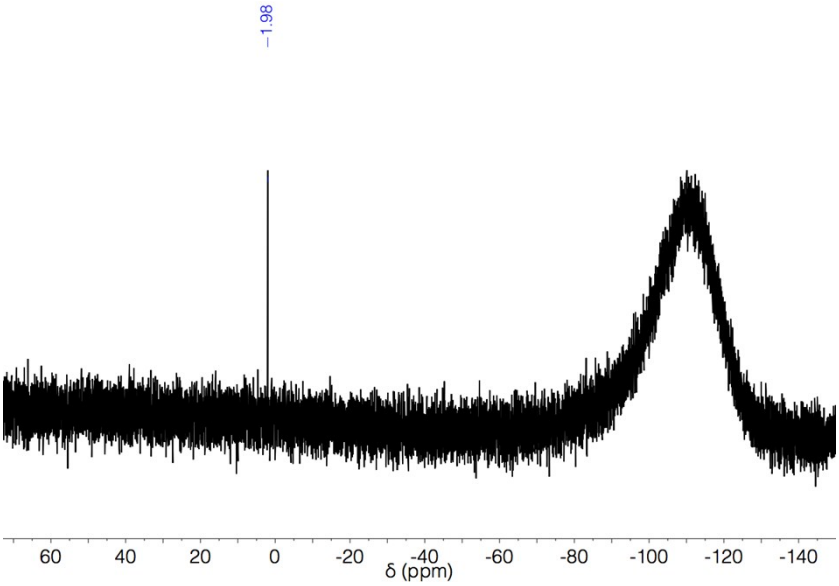

Figure S3 ^{29}Si NMR spectrum (C_6D_6, 79.4 MHz, 303 K) of $\mathbf{1_Y}$.

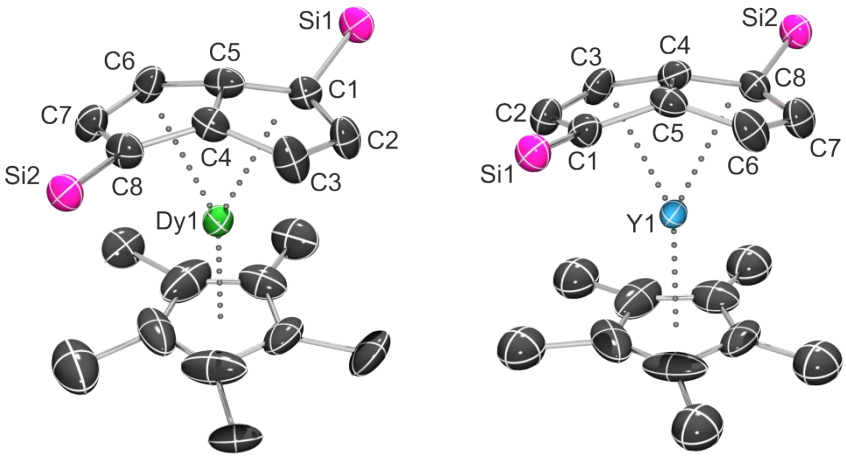

Figure S4 Thermal displacement ellipsoid drawings (50% probability) of $\mathbf{1}_{Dy}$ and $\mathbf{1}_{Y}$. Hydrogen atoms and ^{i}Pr groups mitted for clarity. One part of the disordered Cp* methyl groups is omitted.

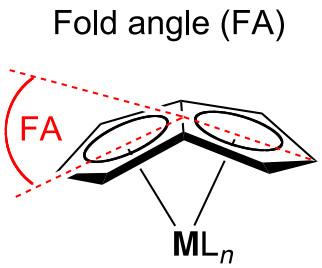

Figure S5 The fold angle (FA) is defined as the dihedral angle between the two C_5 planes.

Table S1 Selected distances (Å) and angles (°) for $\mathbf{1}_{Dy}$ and $\mathbf{1}_{Y}$.

	$\mathbf{1}_{Dy}$	$\mathbf{1}_{Y}$
M–C(1)	2.621(6)	2.628(4)
M–C(2)	2.739(6)	2.736(4)
M–C(3)	2.606(7)	2.585(3)
M–C(4)	2.359(7)	2.357(3)
M–C(5)	2.371(7)	2.369(4)
M–C(6)	2.600(6)	2.603(4)
M–C(7)	2.731(6)	2.736(3)
M–C(8)	2.640(6)	2.620(3)
M–C(Cp*)	2.610(9)-2.643(12)	2.597(7)-2.634(7)
M–Pn$_{cent}$(1)	2.235(3)	2.2295(16)
M–Pn$_{cent}$(2)	2.235(3)	2.2283(18)
M–Cp$_{cent}$	2.344(5)	2.334(3)
(C4–C5)-M-Cp$_{cent}$	169.30(13)	171.06(9)
Fold angle	26.9(4)	27.0(2)

Table S2 Selected experimental crystallographic data.

Structure	**1_{Dy}**	**1_{Y}**
	Crystal data	
Chemical formula	$C_{36}H_{61}DySi_2$	$C_{36}H_{61}Si_2Y$
M_r	712.52	638.93
Crystal system, space group	triclinic, $P\bar{1}$	triclinic, $P\bar{1}$
a, b, c (Å)	9.6968 (5), 12.7898 (6), 16.0392 (7)	9.7114(4), 12.7624(6), 15.9778(8)
α, β, γ (°)	71.948 (4), 75.157 (4), 80.771 (4)	72.103(4), 75.026(4), 80.722(4)
V (Å^3)	1821.05 (16)	1813.26(16)
Z	2	2
μ (mm^{-1})	11.74	3.04
Crystal size (mm)	0.25 × 0.20 × 0.10	0.80 × 0.70 × 0.10
	Data collection	
T_{min}, T_{max}	0.378, 1.000	0.528, 1.000
No. of measured, independent and observed [$I > 2\sigma(I)$] reflections	10563, 6300, 5484	10861, 6770, 6341
R_{int}	0.052	0.044
$(\sin \sigma/\lambda)_{max}$ (Å^{-1})	0.595	0.615
	Refinement	
$R[F^2 > 2\sigma(F^2)]$, $wR(F^2)$, S	0.047, 0.113, 0.88	0.057, 0.154, 0.94
No. of reflections	6300	6770
No. of parameters	398	344
No. of restraints	61	0
$\Delta\rho_{max}$, $\Delta\rho_{min}$ (e Å^{-3})	0.78, -0.94	1.97, -1.10

For all structures: triclinic, $P\bar{1}$, $Z = 2$. Experiments were carried out at 173 K with Cu $K\alpha$ radiation using an Xcalibur, Eos, Gemini ultra. Absorption was corrected for by multi-scan methods, *CrysAlis PRO*, Agilent Technologies, Version 1.171.36.32 (release 02-08-2013 CrysAlis171 .NET) (compiled Aug 2 2013,16:46:58) Empirical absorption correction using spherical harmonics, implemented in SCALE3 ABSPACK scaling algorithm. H-atom parameters were constrained.

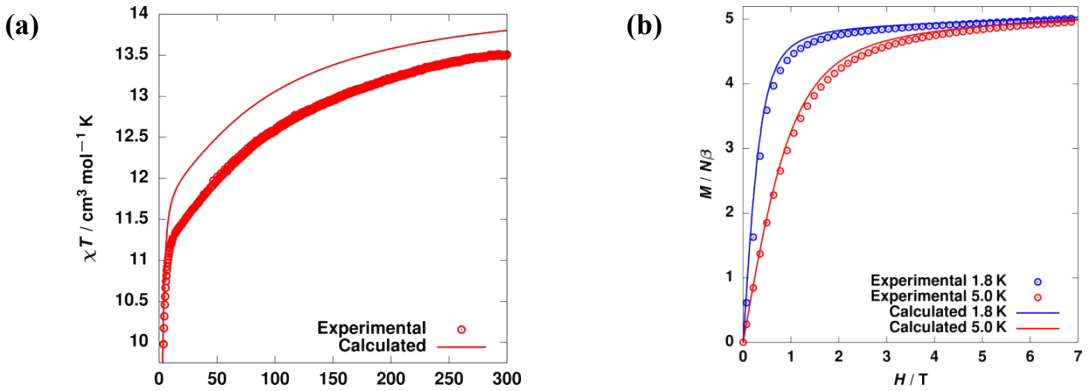

Figure S6 (a) Temperature-dependent magnetic susceptibility acquired in a field of Hdc = 5000 Oe; **(b)** field-dependent isothermal magnetization at 1.8 K and 5.0 K.

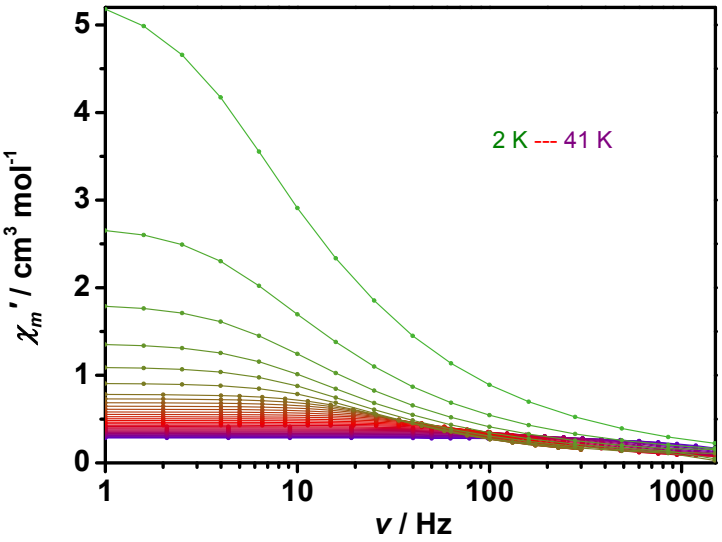

Figure S7 Frequency dependence of the in-phase (χ') AC susceptibility component in zero DC field at different temperatures for $\mathbf{1}_{\mathbf{Dy}}$. The solid lines are a guide for the eye.

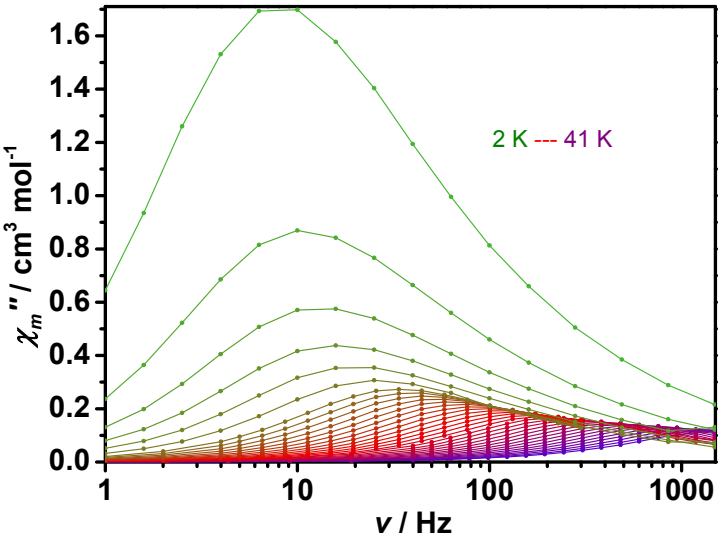

Figure S8 Frequency dependence of the out of phase (χ'') AC susceptibility component in zero DC field at different temperature for $\mathbf{1}_{\mathbf{Dy}}$. The solid lines are a guide for the eye.

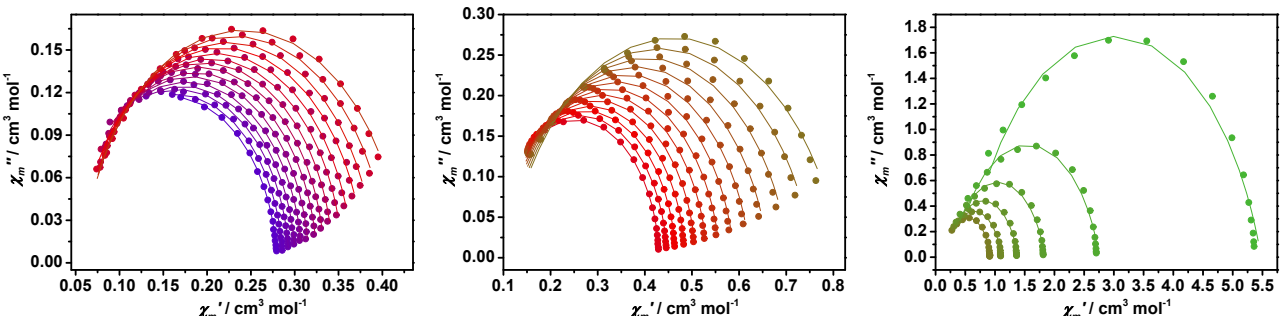

Figure S9 Cole-Cole plot at T = 41-27 K (left), T = 26-14 K (centre) and T = 12-2 K (right) using the AC susceptibility data for $\mathbf{1}_{\mathbf{Dy}}$. The solid lines are the best fits obtained with a generalized Debye model.

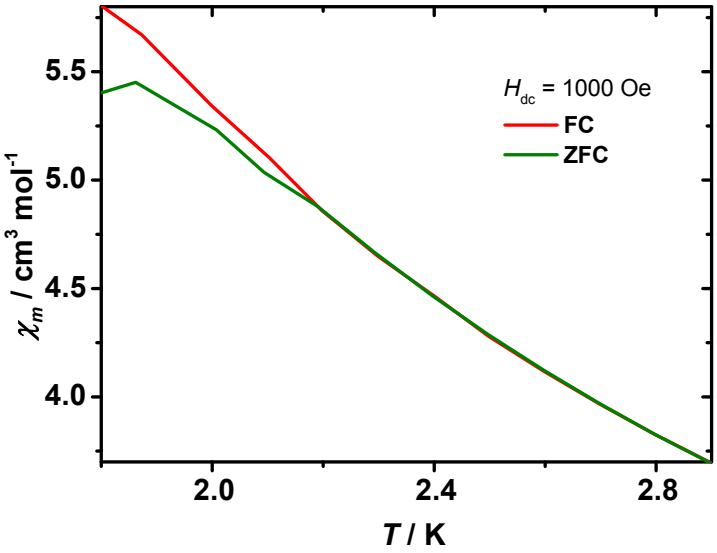

Figure S10 Field-cooled (green) and zero-field-cooled (red) variable-temperature magnetic susceptibility for $\mathbf{1}_{\mathbf{Dy}}$ at 1000 Oe in warming mode (2 K/min).

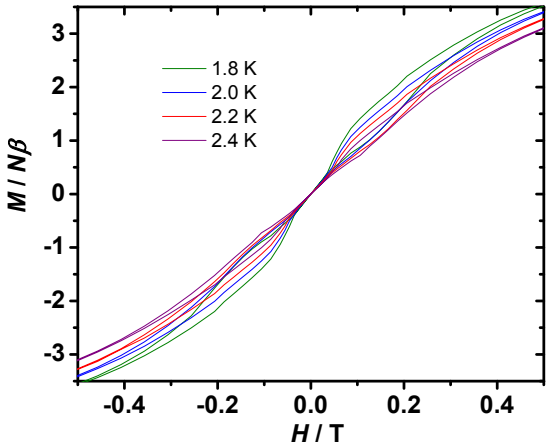

Figure S11 Magnetization vs. field hysteresis for $\mathbf{1}_{\mathbf{Dy}}$ under an average sweep rate of 6.6 Oe s^{-1}.

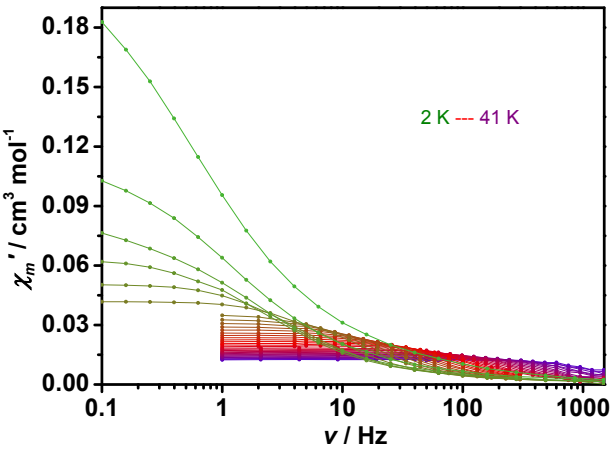

Figure S12 Frequency dependence of the in-phase (χ') AC susceptibility component in zero DC field at different temperatures for $\mathbf{Dy@1}_{\mathbf{Y}}$. The solid lines are a guide for the eye.

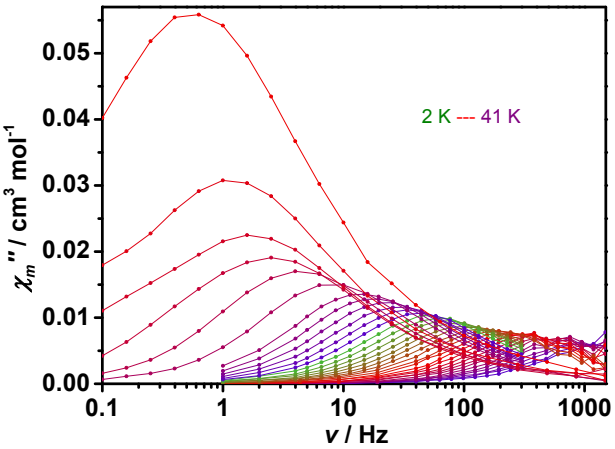

Figure S13 Frequency dependence of the out of phase (χ'') AC susceptibility component in zero DC field at different temperature for **Dy@1$_Y$**. The solid lines are a guide for the eye.

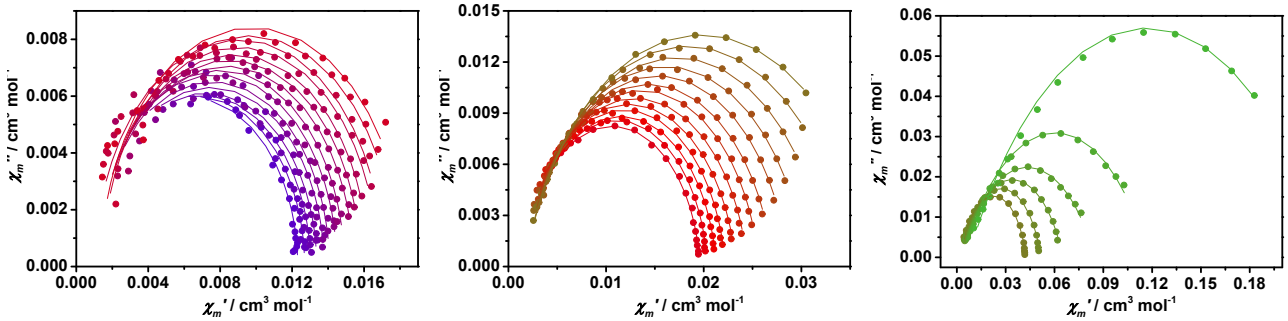

Figure S14 Cole-Cole plot at T = 41-27 K (left), T = 26-14 K (centre) and T = 12-2 K (right) using the ac susceptibility data for **Dy@1$_Y$**. The solid lines are the best fits obtained with a generalized Debye model.

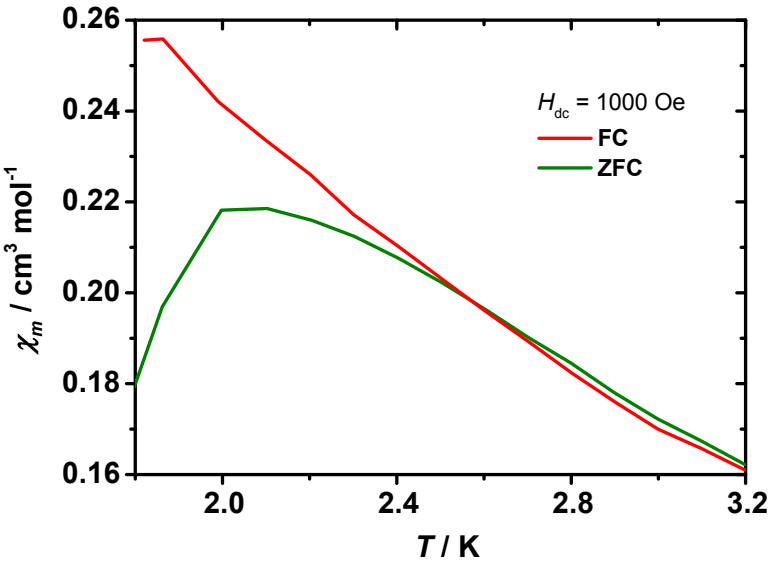

Figure S15 Field cooled (FC, green) and zero-field-cooled (ZFC, red) variable-temperature magnetic susceptibility for **Dy@1$_Y$** at 1000 Oe in warm mode (2 K/min).

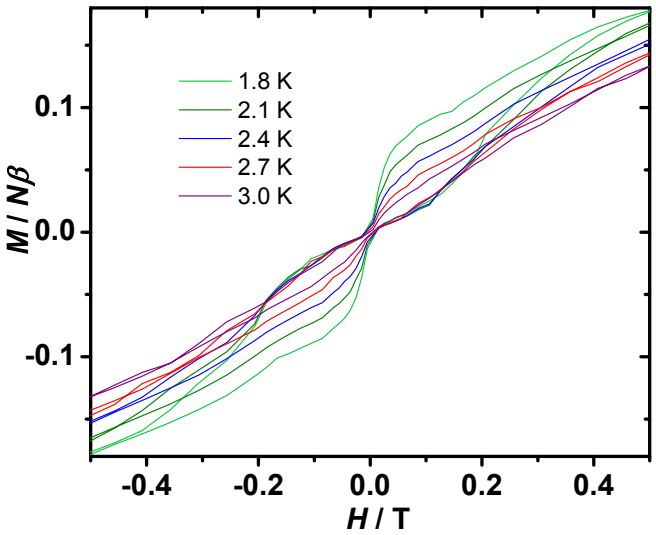

Figure S16 Hysteresis for **Dy@1$_Y$** under an average field sweep rate of 9.8 Oe s^{-1}.

Computational Details

The geometry of $\mathbf{1_{Dy}}$ was extracted from the crystal structure. Positions of hydrogen atoms were optimized at DFT level using the pure GGA PBE exchange correlation functional[9] while the positions of the heavier atoms were kept frozen to their respective crystal structure coordinates. The Dy^{3+} ion was replaced by Y^{3+} in the geometry optimizations to avoid convergence problems. Ahlrichs' def2-SVP basis sets were used in all DFT calculations. The core electrons of Y were treated with an effective core potential (ECP).[10] The DFT calculations were carried out using the Orca 4.0.0 code.[11]

The multi-reference *ab initio* calculations were performed using the standard CASSCF/SO-RASSI methodology as implemented in the Molcas quantum chemistry code versions 8.0 and 8.2.[12] Scalar relativistic effects were treated using the exact two component (X2C) transformation.[13] Roos' ANO-RCC basis sets were employed in all multireference calculations. A VQZP quality basis set corresponding to a [9s8p6d4f3g2h] contraction was used for Dy^{3+}, VTZP basis sets corresponding to [4s3p2d1f] and [3s2p1d] contractions were used for the C and H atoms in the cyclopentadienyl and pentalene cores, respectively, and VDZP quality basis sets corresponding to [4s3p1d], [3s2p1d], and [2s1p] contractions were used for the Si, and other C and H atoms, respectively.[14] A state-averaged CASSCF calculation[15] correlating all nine 4f electrons in the seven 4f orbitals was performed. All 21 sextets, 224 doublets, and 490 doublets were solved. The lowest 21 sextets, 128 quartets, and 130 doublets (corresponding to an energy cut-off of 50,000 cm^{-1}) were mixed by spin-orbit coupling using the restricted active space state interaction (SO-RASSI) method.[16] All spin 21 spin-sextets were included in the SO-RASSI procedure. The local magnetic properties (**g** tensor, crystal field parameters, magnetic susceptibility, magnetization, and transition magnetic moments) were then extracted from the SO-RASSI wave functions using the SINGLE_ANISO routine.[17-19]

Table S3 Properties of the eight lowest Kramers' doublets in the ground $^6H_{15/2}$ multiplet of $\mathbf{1_{Dy}}$.

KD	E / cm^{-1}	g_x	g_y	g_z	θ[a]
1	0	0.0024	0.0040	19.3900	
2	197	0.0251	0.0277	16.5060	4.0°
3	375	0.1234	0.1492	14.1861	3.3°
4	498	0.5948	0.7648	11.4585	1.1°
5	581	4.1225	4.2798	7.6541	16.4°
6	642	2.6966	5.0779	10.9892	90.7°
7	744	0.2216	0.4375	16.5020	91.5°
8	1000	0.0042	0.0081	19.8478	88.6°

[a] The angle between the principal axis of the doublet and the principal axis of the ground doublet.

Table S4 *Ab initio* calculated crystal-field parameters for $\mathbf{1_{Dy}}$.

k	q	$B(k,q)$
2	– 2	-0.297232
2	– 1	0.208131
2	0	-4.588615
2	1	0.483546
2	2	3.894423
4	– 4	-0.000472
4	–3	-0.001782
4	–2	0.001115
4	–1	-0.001247
4	0	0.001066
4	1	-0.003708
4	2	0.007971
4	3	-0.000507
4	4	0.007354
6	–6	-0.000007
6	–5	0.000039
6	–4	0.000011
6	–3	-0.000012
6	–2	0.000024
6	–1	-0.000013
6	0	-0.000014
6	1	-0.000076
6	2	0.000221
6	3	-0.000252
6	4	-0.000171
6	5	0.000379
6	6	0.000052

Table S5 Squared projections of the 16 lowest states (belonging to the eight lowest KDs) of $\mathbf{1}_{\mathbf{Dy}}$ onto $|JM_J\rangle$ states where $J = 15/2$.

	KD1		**KD2**		**KD3**		**KD4**		**KD5**		**KD6**		**KD7**		**KD8**	
$M_J = -15/2$	0.925	0.000	0.001	0.000	0.000	0.072	0.000	0.001	0.001	0.000	0.000	0.000	0.000	0.000	0.000	0.000
$M_J = -13/2$	0.001	0.000	0.888	0.000	0.000	0.002	0.000	0.105	0.000	0.000	0.000	0.002	0.000	0.000	0.000	0.000
$M_J = -11/2$	0.068	0.000	0.001	0.000	0.000	0.808	0.000	0.006	0.101	0.000	0.007	0.002	0.004	0.001	0.001	0.000
$M_J = -9/2$	0.002	0.000	0.099	0.000	0.000	0.007	0.000	0.731	0.004	0.010	0.014	0.091	0.002	0.032	0.005	0.002
$M_J = -7/2$	0.004	0.000	0.003	0.000	0.000	0.098	0.000	0.011	0.560	0.004	0.116	0.017	0.137	0.011	0.034	0.004
$M_J = -5/2$	0.000	0.000	0.007	0.000	0.000	0.001	0.000	0.129	0.003	0.006	0.036	0.340	0.029	0.313	0.057	0.079
$M_J = -3/2$	0.000	0.000	0.000	0.000	0.000	0.010	0.001	0.000	0.247	0.001	0.027	0.001	0.380	0.012	0.223	0.098
$M_J = -1/2$	0.000	0.000	0.000	0.000	0.000	0.001	0.000	0.015	0.003	0.059	0.025	0.321	0.005	0.075	0.160	0.336
$M_J = 1/2$	0.000	0.000	0.000	0.000	0.001	0.000	0.015	0.000	0.059	0.003	0.321	0.025	0.075	0.005	0.336	0.160
$M_J = 3/2$	0.000	0.000	0.000	0.000	0.010	0.000	0.000	0.001	0.001	0.247	0.001	0.027	0.012	0.380	0.098	0.223
$M_J = 5/2$	0.000	0.000	0.000	0.007	0.001	0.000	0.129	0.000	0.006	0.003	0.340	0.036	0.313	0.029	0.079	0.057
$M_J = 7/2$	0.000	0.004	0.000	0.003	0.098	0.000	0.011	0.000	0.004	0.560	0.017	0.116	0.011	0.137	0.004	0.034
$M_J = 9/2$	0.000	0.002	0.000	0.099	0.007	0.000	0.731	0.000	0.010	0.004	0.091	0.014	0.032	0.002	0.002	0.005
$M_J = 11/2$	0.000	0.068	0.000	0.001	0.808	0.000	0.006	0.000	0.000	0.101	0.002	0.007	0.001	0.004	0.000	0.001
$M_J = 13/2$	0.000	0.001	0.000	0.888	0.002	0.000	0.105	0.000	0.000	0.000	0.002	0.000	0.000	0.000	0.000	0.000
$M_J = 15/2$	0.000	0.925	0.000	0.001	0.072	0.000	0.001	0.000	0.000	0.001	0.000	0.000	0.000	0.000	0.000	0.000

References

1. F. G. N. Cloke, M. C. Kuchta, R. M. Harker, P. B. Hitchcock and J. S. Parry, *Organometallics*, 2000, **19**, 5795.
2. Agilent Technologies, *CrysalisPro 1.171.36.32*, 2011.X
3. (a) R. H. Blessing and D. A. Langs, *J. Appl. Crystallogr*., 1987, **20**, 427. (b) R. H. Blessing, *Acta Crystallogr., A, Found. Crystallogr*., 1995, **51**, 33.
4. P. T. Beurskens, G. Beurskens, R. Gelder, J. M. M. Smits, S. de Garcia-Granda, and R. O. Gould, 2008. The *DIRDIF2008* program system, Crystallography Laboratory, University of Nijmegen, The Netherlands.
5. L. Palatinus and G. Chapuis, *J. Appl. Crystallogr.*, 2007, **40**, 786.
6. G. M. Sheldrick, *Acta Crystallogr., A,* 2008, **64**, 112.
7. O. V. Dolomanov, L. J. Bourhis, R. J. Gildea, J. A. K. Howard and H. Puschmann, *J. Appl. Crystallogr.*, 2009, **42**, 339.
8. O. V. Dolomanov, L. J. Bourhis, R. J. Gildea, J. A. K. Howard and H. Puschmann, *J. Appl. Crystallogr.*, 2009, **42**, 339.
9. (a) J. P. Perdew, K. Burke, M. Ernzerhof. *Phys. Rev. Lett.*, **1996**, *77*, 3865; (b) J. P. Perdew, K. Burke, M. Ernzerhof. *Phys. Rev. Lett.*, 1996, **78**, 1396.
10. (a) F. Weigend, R. Ahlrichs. *Phys. Chem. Chem. Phys.*, 2005, **7**, 3297; (b) A. Schäfer, H. Horn, R. Ahlrichs. *J. Chem. Phys.*, 1992, **97**, 2571.
11. F. Neese. *WIREs Comput. Mol. Sci.*, 2017, **8***,* e1327.
12. F. Aquilante, J. Autschbach, R. K. Carlson, L. F. Chibotaru, M. G. Delcey, L. De Vico, I. Fdez. Galván, N. Ferré, L. M. Frutos, L. Gagliardi, M. Garavelli, A. Giussani, C. E. Hoyer, G. Li Manni, H. Lischka, D. Ma, P. Å. Malmqvist, T. Müller, A. Nenov, M. Olivucci, T. B. Pedersen, D. Peng, F. Plasser, B. Pritchard, M. Reiher, I. Rivalta, I. Schapiro, J. Segarra-Martí, M. Stenrup, D. G. Truhlar, L. Ungur, A. Valentini, S. Vancoillie, V. Veryazov, V. P. Vysotskiy, O. Weingart, F. Zapata, R. Lindh, *J. Comp. Chem.*, 2016, **37**, 506.
13. (a) W. Kutzelnigg, W. Liu. *J. Chem. Phys.*, 2005, **123**, 241102; (b) P. Daoling, M. Reiher. *Theor. Chem. Acc.,* 2012, **131**, 1.
14. (a) K. Andersson, P. Å. Malmqvist, B. O. Roos. *J. Chem. Phys.*, **1992**, *96*, 1218; (b) B. O. Roos, R. Lindh, P. Å. Malmqvist, V. Veryazov, P.-O. Widmark. *J. Phys. Chem. A*, **2004**, *108*, 2851; (c) B. O. Roos, R. Lindh, P. Å. Malmqvist, V. Veryazov, P.-O. Widmark, A. C. Borin. *J. Chem. Phys. A*, 2008, **112**, 11431.
15. (a) B. O. Roos in Advances in Chemical Physics, *Ab Initio Methods in Quantum Chemistry II*, Vol. 69 (Ed.: K. P. Lawley), Wiley, New York, 1987, pp. 399–455. (b) B. O. Roos, R. Lindh, P. Å. Malmqvist, V. Veryazov, P.-O. Widmark. *Multiconfigurational Quantum Chemistry.* Wiley, Hoboken, NJ, 2016.
16. P. Å. Malmqvist, B. O. Roos, B. Schimmelpfenning. *Chem. Phys. Lett.*, 2002, **357**, 230.
17. (a) L. F. Chibotaru, L. Ungur. *J. Chem. Phys.*, 2012, **137**, 064112. (b) L. Ungur, L. F. Chibotaru in Lanthanides and Actinides in Molecular Magnetism. *Computational Modelling of the Magnetic Properties of Lanthanide Compounds*. (Ed.: R. A. Layfield, M. Murugesu), Wiley-VHC, Weinheim, Germany, 2015, pp. 153-184.
18. L. Ungur, L. F. Chibotaru. *Chem. Eur. J.*, 2017, **23**, 3708.
19. L. Ungur, M. Thewissen, J.-P. Costes, W. Wernsdorfer, L. F. Chibotaru. *Inorg. Chem.*, 2013, **52**, 6328.